Journal of Molecular Liquids 396 (2024) 123973

Contents lists available at ScienceDirect

Journal of Molecular Liquids

journal homepage: www.elsevier.com/locate/molliq

Mimicking the inner mitochondrial membrane with curved supported lipid bilayers: A neutron reflectometry study

Alessandra Luchini [a,*], Yuri Gerelli [b], Philipp Gutfreund [c], Giovanna Fragneto [c,d], Luigi Paduano [e], Giuseppe Vitiello [e]

[a] Department of Physics and Geology, University of Perugia, Via Alessandro Pascoli, 06123 Perugia, Italy
[b] Institute for Complex Systems, National Research Council and Sapienza University of Rome, Piazzale Aldo Moro 5, 00185 Rome, Italy
[c] Institut Laue-Langevin, 71 avenue des Martyrs, CS 20156, 38042 Grenoble, France
[d] European Spallation Source ERIC, Partikelgatan 2, P.O. Box 176, SE-221 00 Lund, Sweden
[e] Department of Chemical Science, University of Naples "Federico II", Strada Comunale Cinthia, 26, 80126 Napoli, Italy

ARTICLE INFO

Keywords:
Cardiolipin
Buckled membranes
Membrane curvature
Neutron reflectometry
Supported lipid bilayers
Inner mitochondrial membrane

ABSTRACT

Cardiolipin (CL) is a phospholipid with an unusual molecular structure exhibiting four acyl chains bound to a polar headgroup. CL is found in curved regions within biological membranes, such as the poles of cylindrically shaped bacteria and the cristae in mitochondria. Like bacterial cells, mitochondria are characterised by two cell membranes. CL is exclusively found in the inner membrane of mitochondria (IMM), and it is vital for the proper functioning of this organelle. Together with CL, phosphatidylcholine (PC) and phosphatidylethanolamine (PE) are the main lipid components of the IMM. Interestingly, most of the CL in human tissues exhibits C18 acyl chains and alterations of its molecular structure are related to severe diseases. Here we investigated supported lipid bilayers (SLBs) composed of PC, PE and CL as model systems mimicking the IMM. In our experiments we used tetra-oleyl cardiolipin (TOCL), which exhibits four C18 acyl chains and is therefore close to the CL normally present in the IMM, and tetra-myristoyl cardiolipin (TMCL), which exhibits considerably shorter acyl chains, i.e. C14. All samples were investigated both in the presence and in the absence of Ca^{2+} ions. The structure of the produced samples was characterised by neutron reflectometry (NR). Our data indicate that all samples with TMCL were organised as a regular SLB with a small impact of TMCL on the bilayer structure. On the other hand, at a TOCL concentration above 10% mol and upon injection of Ca^{2+}, we observed a large structural rearrangement of the initially formed SLB compatible with the formation of curved bilayer regions that protrude towards the bulk solvent. To the best of our knowledge, this is the first example where specular NR and off-specular scattering revealed buckled SLBs. This experimental evidence indicates the crucial role of CL acyl chain composition in favouring the proper folding of the IMM.

1. Introduction

Cardiolipin (CL) is a glycerophospholipid found both in eukaryotic and prokaryotic cell membranes [1]. Its chemical structure includes two phosphatidyl moieties with a total of four acyl chains of variable length and level of unsaturation, which are bound to a single glycerol unit. Therefore, CL is characterised by a large hydrophobic region and a relatively small polar headgroup resulting in a conical molecular shape. In fact, most of the glycerophospholipids composing biological membranes present only two acyl chains and have often a cylindrical shape [2]. CL is mostly found in the bacterial cytoplasmic membrane and in the inner membrane of mitochondria [3]. Because of its peculiar shape, CL can be accommodated within membrane regions characterised by high curvature, such as the poles of cylindrically shaped bacteria [4], and the cristae in mitochondria [5]. Mitochondria are characterised by two cell membranes, and CL is exclusively present in the inner mitochondrial membrane (IMM), where it contributes to the proper functioning of this vital organelle [5]. CL is asymmetrically distributed between the two IMM leaflets and it is mostly localized in the inner leaflet [6]. This asymmetric distribution results in regions of the IMM with negative curvature, which protrude towards the cytoplasm [7]. CL not only participates in the structural architecture of the IMM, but it contributes

* Corresponding author.
E-mail address: alessandra.luchini@unipg.it (A. Luchini).

https://doi.org/10.1016/j.molliq.2024.123973
Received 20 November 2023; Received in revised form 2 January 2024; Accepted 3 January 2024
Available online 9 January 2024

also to the biological function of different membrane proteins [8,9]. Furthermore, CL is a signaling molecule: under stress conditions, its exposure in the outer mitochondrial membrane is part of the apoptotic signaling pathway [10]. Reduced levels of CL, or aberrant CL structure and localization, are likened to neuronal dysfunction and are associated with severe neurodegenerative disease such as Alzheimer's disease, Parkinson's disease, and Barth syndrome [11]. Because of its role in these pathologies, CL is considered a potential pharmaceutical target for therapies against neurodegenerative diseases [12,11]. The biological importance of CL for human health together with its peculiar structure have promoted several studies to understand its self-assembly properties. In aqueous environments, CL can organise into different kinds of lipid phases depending on temperature, ionic strength, and the presence of divalent cations such as calcium ions (Ca^{2+}) [13–15]. Such lipid phases include both the lamellar and the non-lamellar inverse hexagonal phases [16]. Binary mixtures of CL and other phospholipids, such as phosphatidylcholine (PC), phosphatidylethanolamine (PE) and phosphatidylglycerol (PG), have mostly been investigated as models of bacterial and mitochondrial membranes [17,13,14,9,18,19]. Fewer studies have investigated more complex mixtures, including additional phospholipids [20,21].

The IMM is characterised by three main lipid components which are PC, PE and CL [22]. The fatty acid composition of these lipids including CL is extremely variable depending on the specific tissue, although C18 acyl chains are the most abundant in tissues such as the heart, skeletal muscles, and liver [23]. While PC and PE are the most abundant lipid component, the concentration of CL is typically in the range 5-20 mol% [24]. Lipid bilayers formed by ternary mixtures of PC, PE and CL have been mostly investigated with computational methods [25–27]. These studies have indicated that these mixtures could arrange into a lamellar phase and CL was found to have a small impact on the bilayer structure, whereas it mostly affected the bilayer fluidity and lipid lateral diffusion [25]. Depending on environment conditions, such as the presence of divalent ions, the bilayer with CL was found to stabilize buckled regions [26,27].

Here we discuss an experimental study of supported lipid bilayers (SLBs) composed of 1-palmitoyl-2-oleoyl-glycero-3-phospho-choline (POPC), 1-palmitoyl-2-oleoyl-glycero-3-phospho-ethanolamine (POPE) and CL by means of neutron reflectometry (NR) measurements, a non-destructive technique that can provide structural information with a few Å resolution and is particularly suitable for the characterisation of biological membranes [28]. We studied SLBs with two different kinds of CL and varied both the CL concentration and the composition of the buffer. For our experiments we used tetra-oleyl cardiolipin (TOCL), which is composed by four C18 acyl chains and is therefore close to the CL normally present in the IMM. We compared the results obtained for the TOCL SLBs with those obtained for SLBs prepared with another CL species, i.e. tetra-myristoyl cardiolipin (TMCL). TMCL presents shorter acyl chains, i.e. C14, and is not abundant in the IMM. These experiments were aimed at understanding the role of the acyl chain composition of CL in determining the structure of the bilayer. In addition, the SLBs with both TOCL and TMCL were characterised in the presence and in the absence Ca^{2+} ions. By performing both specular and off-specular NR experiments we revealed remarkable differences in the SLBs produced with TOCL and TMCL, which supports the crucial importance of the long and unsaturated acyl chains of the CL in favouring the formation of high-curvature regions in the IMM.

2. Materials and methods

2.1. Chemicals

1-palmitoyl-2-oleoyl-glycero-3-phosphocholine (POPC) (≥ 99% purity), 1-palmitoyl-2-oleoyl-sn-glycero-3-phosphoethanolamine (POPE) (≥ 99% purity), 1,3'-bis(1,2-dimyristoyl-sn-glycero-3-phospho)-glycerol (TMCL), and 1',3'-bis[1,2-dioleoyl-sn-glycero-3-phospho]-glycerol (TOCL) were purchased from Avanti Polar Lipids, Inc. (Alabaster, AL) and used without further purification. Heavy water (D2O 99.9% purity), chloroform (≥ 99.5% purity), ethanol (98% purity), acetone (98% purity), were purchased from Sigma-Aldrich.

2.2. Supported lipid bilayer preparation

Supported lipid bilayers (SLBs) were produced *via* vesicle fusion. Lipid films with the selected POPC/POPE/TMCL or POPC/POPE/TOCL ratios were prepared by mixing POPC, POPE, TMCL or POPC, POPE, TOCL solution in chloroform and subsequently evaporating the solvent under nitrogen flow. All films were prepared using a total amount of lipids of 4 mg. The lipid films were rehydrated with 2 ml of 20 mM HEPES buffer (100 mM NaCl, 20 mM KCl, pH = 7.4), both in the absence and in the presence of 5 mM $CaCl_2$. The lipid suspensions with final lipid concentration 2 mg/ml were sonicated with a tip sonicator for 5 minutes and used immediately after for the formation of the SLBs. Vesicle solutions were injected in the cell, including a hydrophilic solid substrate, used on the neutron reflectometer and, after approximately 30 min, pure water was injected to create an osmotic shock and favour the vesicle fusion onto the substrate. Before collecting the experimental data, the buffer, either with or without $CaCl_2$, was reintroduced into the cell.

2.3. Neutron reflectometry

Neutron Reflectometry (NR) experiments were performed on the FIGARO reflectometer [29] at the Institut Laue-Langevin (ILL), Grenoble (France). FIGARO is a vertical scattering plane, time-of-flight reflectometer. Two incoming angles, namely 0.8° and 3.2°, were used to collect data in the q-range $0.003\ Å^{-1} < q < 0.25\ Å^{-1}$. The reflected intensity measured on FIGARO was converted to an absolute specular reflectivity scale (R(q)) by normalisation to the direct beam measured at the same slit settings. Slits were chosen to vary with the incident angle in such a way as to provide a constant illumination of the sample (35 × 65 mm). The background was measured on the top side of the reflectivity signal, in a region where negligible off-specular scattering was observed, and subtracted from the measured reflected intensity. The neutron beam is focused on a solid/liquid cell containing the solid support and the sample. Monocrystalline silicon supports (80 mm x 50 mm x 15 mm) were cleaned with sequential sonication (~ 20 min) in chloroform, ethanol, and acetone followed by a 3 min treatment with a plasma cleaner. The freshly cleaned silicon supports were assembled in the solid/liquid cells. 2 ml of the sample were introduced into the solid/liquid cells through manual injection with a syringe. The temperature of the solid/liquid cells was kept at 25 °C during data collection with a thermalized water bath.

In order to obtain different contrasts between the samples and the solvents, NR measurements were performed with three buffers (100 mM NaCl, 20 mM KCl, 5 mM $CaCl_2$, $pH = 7.4$) prepared in 100% D_2O (named D_2O-buffer, $\rho = 6.35 \cdot 10^{-6}\ Å^{-2}$), 38% D_2O 62%H_2O (named SMW-buffer, $\rho = 2.07 \cdot 10^{-6}\ Å^{-2}$) and 100% H_2O (named H_2O-buffer, $\rho = -0.56 \cdot 10^{-6}\ Å^{-2}$). 20 ml of buffer were injected with a HPLC pump and 1 ml/min flow rate to achieve contrast exchange. Data collected in the different contrasts were simultaneously analysed with the same structural model.

2.3.1. Specular NR data analysis

NR data were analysed with an in-house developed code that is based on the Parratt formalism [30] to calculate the reflectivity profile corresponding to a given structural model. The sample is considered to be composed by a stack of layers, each with a different thickness (t), scattering length density (ρ), solvent volume fraction (ϕ_s) and surface roughness (σ). The scattering length density, ρ, is defined as

$$\rho = \sum_i \frac{n_i b_i}{V_m} \quad (1)$$

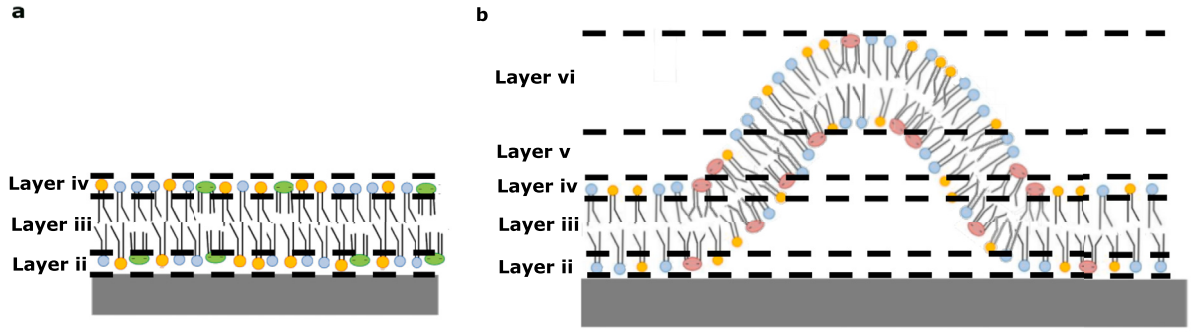

Fig. 1. Schematic representation of the models used to analyse the specular neutron reflectometry data in case of supported lipid bilayers (a) and supported lipid bilayers with curved regions protruding towards the bulk solvent (b).

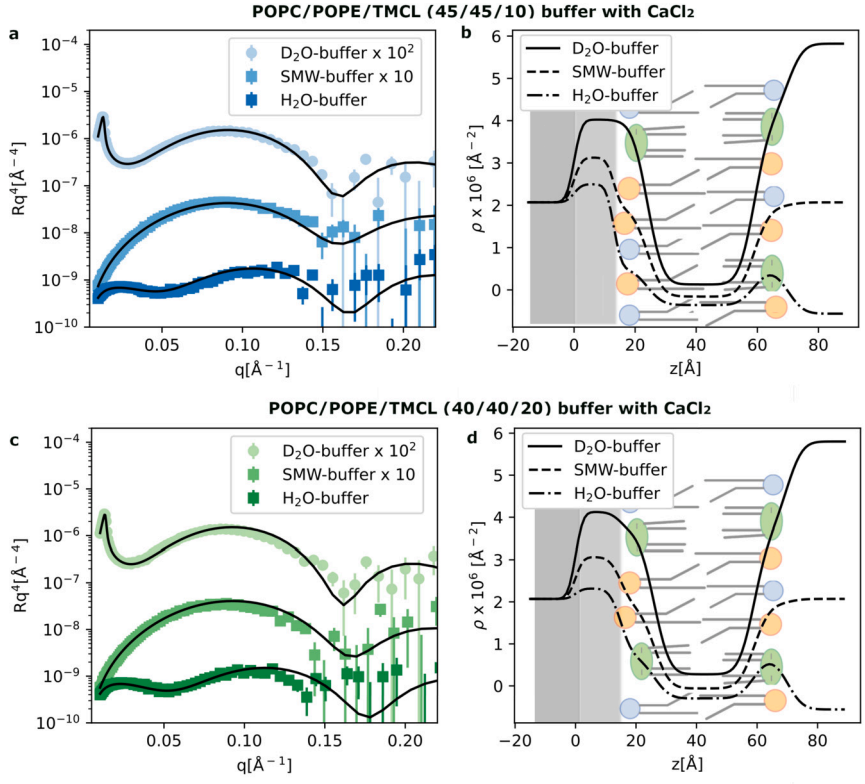

Fig. 2. Specular NR data and corresponding fitting curves for the PC/PE/TMCL SLBs in buffer with Ca^{2+} (a-c). Data are scaled in order to improve visualisation. Scattering length density profiles, $\rho(z)$, obtained from data analysis (b-d).

where n_i is the number of i-type nuclei and b_i is the corresponding coherent scattering length, while V_m is the molecular volume. In the case of the phospholipids used in this study, we estimated the scattering length density corresponding to the headgroups and acyl chains by using prior information on the headgroup and acyl chain molecular volume and the corresponding chemical composition. In the case of POPC and POPE, X-ray scattering was used to assess the molecular volume of the headgroups and acyl chains for pure POPC and POPE bilayers [31,32]. Based on the values obtained, POPC and POPE result in similar acyl chain molecular volumes corresponding to 925 $Å^3$, whereas the molecular volumes for the PC and the PE headgroups are 331 $Å^3$ and 245 $Å^3$, respectively. In the case of TMCL and TOCL, to the best of our knowledge, there are no experimental data available on their molecular volumes. Therefore, we made an estimation based on their molecular structures leading to 1942 $Å^3$ and 1794 $Å^3$, respectively, for the TOCL and TMCL acyl chains and 391 $Å^3$ for the CL headgroup. These values were used to estimate an initial guess of the lipid scattering length density, which was subsequently optimised to fit the experimental data.

In this study, we used two different models to analyse the collected specular NR data. Fig. 1a shows the standard bilayer model used to interpret the data collected for all SLBs with TMCL (both in the presence and in the absence of Ca^{2+} ions). This model includes 4 layers: i) silicon oxide (not shown in the cartoons), ii) inner lipid headgroups; iii) acyl chains; iv) outer lipid headgroups. Fig. 1b shows the model used for the SLBs with TOCL above 10% mol and in the presence of Ca^{2+} ions. Two additional layers were included on top of the outer lipid headgroups (i.e. layer iv): v) first lipid layer; vi) second lipid layer. Layers v and vi were used to describe the curved bilayer region protruding from the support surface towards the bulk solvent. Addition of a larger number of layers to describe these curved bilayer regions was not found to improve the fit quality. Upon the first optimisation of the model parameters the scattering length density of layer v) and vi) was fixed to the theoretical value for the investigated lipid mixtures (further details in the Results and Discussion section).

2.3.2. Off-specular scattering data analysis

Off-specular scattering was analysed according to the algorithm presented in [33]. The simulation is based on the same model as the specular reflectivity but with Gaussian-shaped in-plane scattering length density (SLD) inhomogeneities assumed in layers ii-vi (Fig. 1b). For layers ii-iv these were assumed to be water inclusions with the same SLD as the bulk water phase and with the same volume fraction as the hydration of the acyl chains. These water inclusions were surrounded by dry acyl chains for layer iii and by rest-hydrated head groups in layers ii and iv, respectively. Layers v and vi were modelled as the inverse situation, inclusions of rest-hydrated lipids, with an averaged SLD not distinguishing heads and tails, at the same volume fraction as the water inclusions underneath, embedded in bulk water with the same correlation length as the flat bi-layer parts underneath. This model has only two free variables, namely the mean size of the buckled parts of the bilayer and the mean size of the flat parts in between.

3. Results and discussion

Fig. 2 shows the specular NR data collected for the PC/PE/TMCL SLBs with TMCL concentration 10 and 20 mol%. SLBs were measured in a physiological buffer in the presence and in the absence of Ca^{2+} ions. The model used to analyse the collected data described the sample structure as a stack of four different layers: i) silicon oxide, which is part of the support structure; ii) inner lipid headgroups; iii) lipid acyl chains; iv) outer lipid headgroups. As the initial optimisation of the model parameters to the experimental data resulted in a very comparable structure for layers ii) and iv), these were later constrained to have the same parameter values in the final analysis, which corresponds to a SLB with a symmetric structure and composition. This approach sensibly reduced the number of fitting parameters in the model. Figs. 2b and 2d show the scattering length density profiles $\rho(z)$ obtained from the data analysis that report on the organisation of the different lipid components, and water molecules, along the direction (z) perpendicular to the bilayer surface. As reported in Table 1, all the investigated PC/PE/TMCL mixtures produced SLBs with similar structure, and with only minor differences as compared to the PC/PE SLB used as a reference in this study (see supplementary material, Fig. S1 and Table S1). In agreement with previous results [20,25], the presence of TMCL caused a slight increase of the thickness of the bilayer and the overall SLB structure was not remarkably affected by the presence of Ca^{2+} in the buffer (Figs. S2 and S3). The increase in the bilayer thickness is associated with the condensing effect of the CL molecules on the surrounding phospholipid molecules. No further significant variation was observed when the TMCL concentration was increased to 30% mol both in the presence and in the absence of Ca^{2+} (Figs. S4 and S5).

Fig. 3 shows the specular NR data collected for the PC/PE/TOCL SLBs with a TOCL concentration of 10 and 20 mol%. As for TMCL, these SLBs were characterised both in the presence and in the absence of Ca^{2+} in the buffer. At TOCL concentration 10 mol%, the collected data showed a similar trend as the data in Fig. 2 and the same model discussed above was successfully implemented to analyse the experimental data. The structural parameters reported in Tables 1 and 2 indicate that at 10 mol% TOCL or TMCL, mixed with POPC and POPE, form SLBs with similar structure. At TOCL concentration 20 mol% we observed once again a bilayer structure similar to that obtained for TOCL at 10 mol% in the absence of Ca^{2+} (Fig. 3c), whereas relevant structural changes were detected in the presence of Ca^{2+} ions as indicated by the increase in reflectivity in the mid-q range (Fig. 3e). This remarkable variation was observed both when the buffer with Ca^{2+} was used directly for the SLB formation, and when Ca^{2+} ions were added separately after the SLB was formed in the absence of Ca^{2+} (Fig. 3c). This evidence indicates that the observed structural change is induced by the injection of Ca^{2+} and can take place also in already formed SLBs. Similar data were collected when the TOCL concentration was further increased to 30 mol% (Fig. 3g). Also in case of the SLB with TOCL 30

Table 1
Optimised parameters from specular NR data analysis: thickness (t), solvent volume fraction (ϕ_s), scattering length density (ρ). Data were analysed with the bilayer model described in Materials and Methods. Surface roughness was in the range of 3-4 Å for all layers.

POPE/POPC/TMCL (45/45/10) buffer without Ca^{2+}		
Parameters	Headgroups	Acyl chains
t [Å]	10 ± 1	33 ± 2
$\rho \cdot 10^{-6}$ [Å^{-2}]	1.9 ± 0.1	-0.27 ± 0.02
ϕ_s	0.53 ± 0.03	0.12 ± 0.02
POPE/POPC/TMCL (45/45/10) buffer with Ca^{2+}		
Parameters	Headgroups	Acyl chains
t [Å]	9 ± 1	31 ± 1
$\rho \cdot 10^{-6}$ [Å^{-2}]	1.9 ± 0.1	-0.29 ± 0.01
ϕ_s	0.50 ± 0.01	0.04 ± 0.01
POPE/POPC/TMCL (40/40/20) buffer without Ca^{2+}		
Parameters	Headgroups	Acyl chains
t [Å]	11 ± 2	31 ± 1
$\rho \cdot 10^{-6}$ [Å^{-2}]	1.9 ± 0.1	-0.28 ± 0.01
ϕ_s	0.45 ± 0.02	0.05 ± 0.01
POPE/POPC/TMCL (40/40/20) buffer with Ca^{2+}		
Parameters	Headgroups	Acyl chains
t [Å]	9 ± 1	31 ± 1
$\rho \cdot 10^{-6}$ [Å^{-2}]	1.9 ± 0.1	-0.27 ± 0.02
ϕ_s	0.50 ± 0.01	0.04 ± 0.01
POPE/POPC/TOCL (45/45/10) buffer without Ca^{2+}		
Parameters	Headgroups	Acyl chains
t [Å]	10 ± 1	32 ± 3
$\rho \cdot 10^{-6}$ [Å^{-2}]	1.9 ± 0.1	-0.28 ± 0.02
ϕ_s	0.55 ± 0.06	0.05 ± 0.03
POPE/POPC/TOCL (45/45/10) buffer with Ca^{2+}		
Parameters	Headgroups	Acyl chains
t [Å]	9 ± 1	31 ± 1
$\rho \cdot 10^{-6}$ [Å^{-2}]	1.9 ± 0.1	-0.29 ± 0.02
ϕ_s	0.50 ± 0.01	0.04 ± 0.01
POPE/POPC/TOCL (40/40/20) buffer without Ca^{2+}		
Parameters	Headgroups	Acyl chains
t [Å]	20 ± 1	32 ± 1
$\rho \cdot 10^{-6}$ [Å^{-2}]	1.9 ± 0.1	-0.28 ± 0.03
ϕ_s	0.52 ± 0.01	0.02 ± 0.02

Table 2
Optimised parameters from specular NR data analysis: thickness (t), solvent volume fraction (ϕ_s), scattering length density (ρ). Surface roughness was in the range of 3-4 Å for all layers except for lipid layers I and II for which we estimated it of 6 ± 1 Å.

POPE/POPC/TOCL (40/40/20) buffer with Ca^{2+}				
Parameters	Headgroups	Acyl chains	lipid layer I	lipid layer II
t [Å]	10 ± 1	32 ± 1	18 ± 4	45 ± 3
$\rho \cdot 10^{-6}$ [Å^{-2}]	1.9 ± 0.1	-0.29 ± 0.04	0.10	0.10
ϕ_s	0.49 ± 0.04	0.11 ± 0.01	0.90 ± 0.08	0.90 ± 0.02
POPE/POPC/TOCL (35/35/30) buffer with Ca^{2+}				
Parameters	Headgroups	Acyl chains	lipid layer I	lipid layer II
t [Å]	11 ± 1	30 ± 1	20 ± 3	47 ± 2
$\rho \cdot 10^{-6}$ [Å^{-2}]	1.9 ± 0.1	-0.29	0.03	0.10
ϕ_s	0.56 ± 0.03	0.12 ± 0.01	0.75 ± 0.02	0.91 ± 0.01

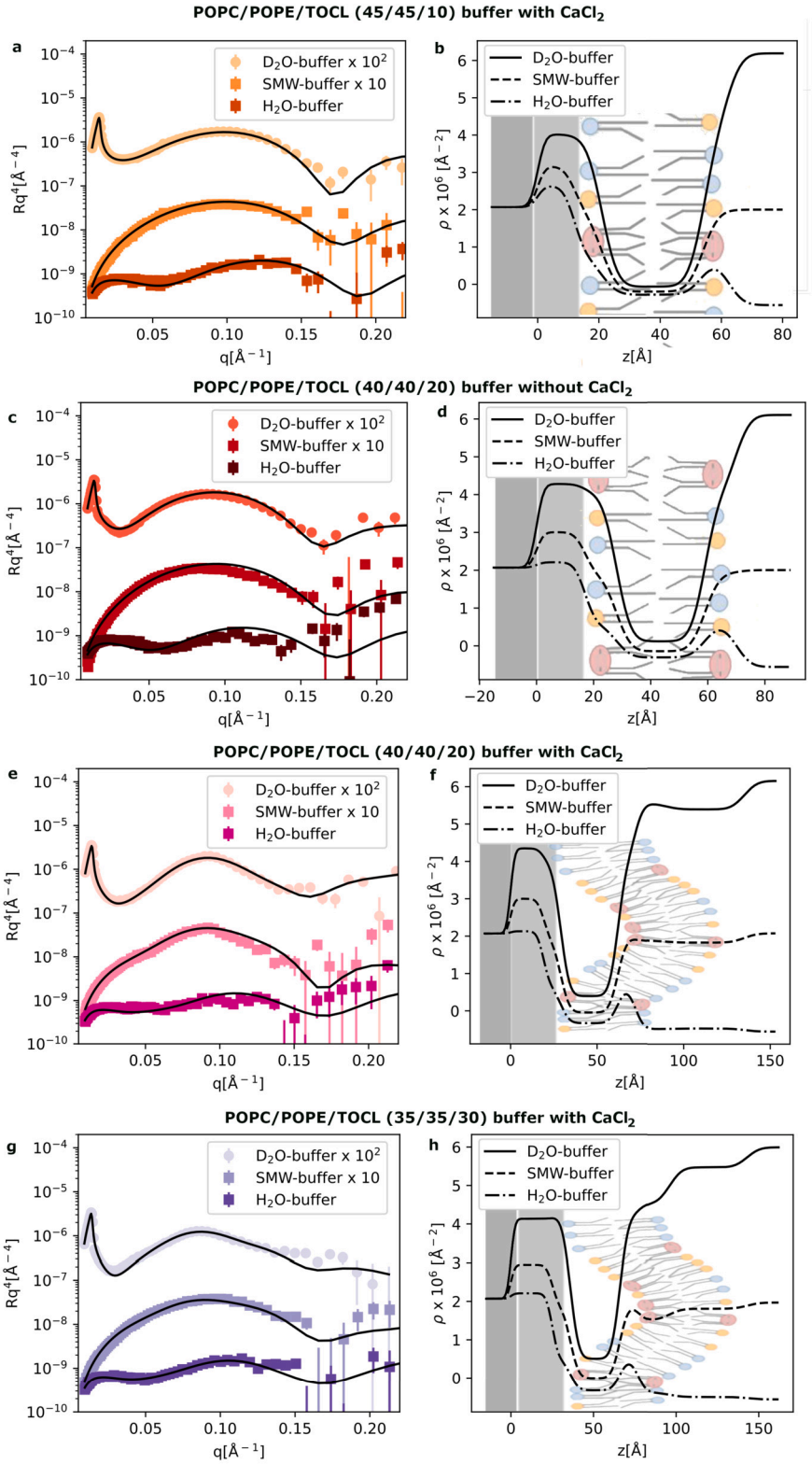

Fig. 3. Specular NR data and the corresponding fitting curves for the PE/PC/TOCL SLBs (a,c,e,g). Data are scaled in order to improve visualisation. Scattering length density profiles obtained from data analysis (b,d,f,h).

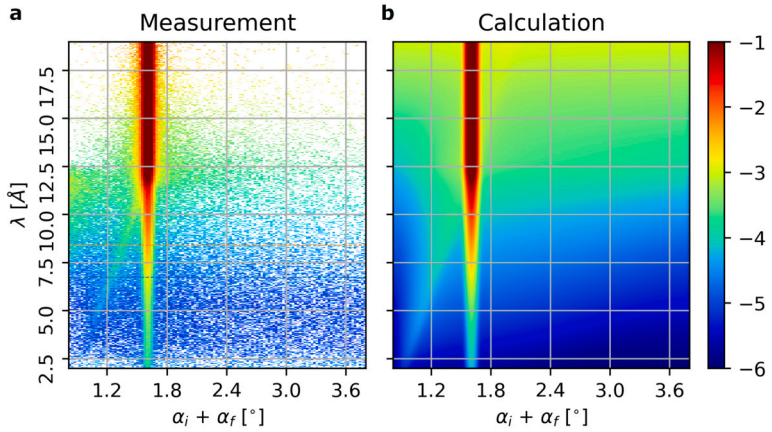

Fig. 4. a) 2D detector image showing the neutron wavelength (λ) as function of the sum of the neutron beam angle before (α_i) and after (α_f) the sample. The intensity is represented by the colour scale on the right side of the figure. b) simulated 2D detector image based on the sample structure model described in the Materials and Methods section.

mol%, the bilayer model could be used successfully to interpret the experimental data in the absence of Ca^{2+} (Fig. S7).

A different model was needed to analyse the data in Fig. 3e and 3g as compared to Fig. 3c (see Materials and Methods). We found that introducing two additional layers with a scattering length density of 0.1×10^{-6} Å^{-2} to the previous model resulted in the best fit of the experimental data. Indeed, this scattering length density value corresponds to the average value expected for the investigated lipid mixtures, as calculated from the molecule chemical structure and molecular volume (see further details in Materials and Methods). During data analysis we optimised the volume fraction, thickness, and surface roughness of these additional layers. As reported in Table 2, our analysis suggests the presence, in the proximity of the silicon substrate, of a lipid bilayer with structure comparable to the SLBs measured in the absence of Ca^{2+}, topped by curved portions of the same bilayer, assumed to protrude further out from the silicon substrate (Fig. 3f and 3h). As a result of the local curvature of the SLB, the lower part resulted characterised by a low surface coverage as indicated by the large solvent volume fraction among the lipid acyl chains. Such structural model agrees with previous computational and experimental studies indicating a larger concentration of CL in the inner leaflet (in this case the one close to the substrate surface), which induced the formation of buckled membrane regions [27,26,34].

Our interpretation of the specular NR data was supported by the analysis of the off-specular scattering. In general, off-specular scattering is produced by lateral mesoscale inhomogenieties in the sample [33]. Off-specular scattering was observed only in the SLBs with TOCL concentration 20 and 30 mol% and in the presence of Ca^{2+}. As shown in Fig. 4a in case of the SLB with TOCL 30 mol% in the presence of Ca^{2+}, the 2D detector image showed a strong specular reflection present at all wavelengths (λ) as indicated by the strong signal located vertically at $\alpha_i + \alpha_f = 1.6°$. The presence of off-specular scattering gives rise to the additional signal visible at $\alpha_i + \alpha_f < 1.6°$, i.e. on the left side of the specular signal. This type of scattering is known as Yoneda scattering [35]. A quantitative interpretation of the off-specular scattering was based on a recently reported approach [33] described in sec. 2. This combined the structural model obtained from the analysis of the specular NR data and included the size and position of the inhomogeneous regions. The result of the calculation is reported in Fig. 4b assuming arbitrarily positioned 20 nm large buckled regions surrounded by 200 nm wide flat regions of the bilayer. The bi-dimensional detector image obtained from such a model is able to reproduce, with exceptional agreement, the experimental data (Fig. 4), indicating the validity of the interpretation as well as of the characteristic size and distances between the buckling portions of the SLB.

A rational explanation for this collective behaviour can be based on the interaction of Ca^{2+} ions and negatively charged CL headgroups. At physiological pH, CL is characterised by a negatively charged headgroup [36]. Ca^{2+} ions can coordinate to the CL headgroups therefore screening the negatively charged groups and favouring clustering of CL in the membrane. Sorting of CL molecules in curved membrane regions is a well-documented phenomenon [19]. On the other hand, CL clustering as driving force for inducing membrane curvature was predicted by computational studies [27,26] but not yet validated experimentally. The analysis of the specular and off-specular NR data presented in this manuscript represents the first experimental evidence of clustering of TOCL and buckling induced in flat SLBs by calcium ions.

While clustering can potentially take place also in case of the SLB with TMCL, interestingly TMCL, which possesses shorter acyl chains than TOCL and they are fully saturated, does not induce the same effect on the membrane structure. This evidence is in agreement with the abundance of long (mostly C18) and unsaturated fatty acyl chains in the IMM, and the strong impact that any modification of the CL molecular structure has on the proper functioning of the mitochondria [37]. In addition, our study also indicates that Ca^{2+} ions have an important role in stabilising the curved regions of the bilayer. The Ca^{2+} concentration is dependent on the status of the cell, and mitochondria play a central role in the regulation of Ca^{2+} concentration [38]. Although membrane proteins are predominantly involved in this regulatory function, other membrane component, such as CL, can also contribute to the Ca^{2+} detection and corresponding response of the mitochondria [39].

4. Conclusions

In eukaryotes, CL is mostly found in the inner membrane of the mitochondria (IMM), a membrane characterised by curved regions, i.e. the cristae, where CL is notably abundant. The analysis of the CL molecular structure in human tissues indicated the prevalence of CL molecules with C18 acyl chains, suggesting a functional role of this specific CL molecular composition in favouring the proper IMM folding [37]. In this study we focused on the role of CL acyl chain length and of Ca^{2+} ions in promoting membrane curvature in SLBs mimicking the IMM. The analysis of specular and off-specular NR data indicated that in the absence of Ca^{2+} ions, SLBs composed by POPC, POPE and TMCL or TOCL have very similar structures, slightly differing only in the total thickness because of the different lipid packing. The structure of the SLBs containing TMCL did not change upon addition of Ca^{2+} at any stage of the measurements. On the contrary, in the presence of TOCL at a concentration above 10 mol%, addition of Ca^{2+} ions on already formed bilayers induced striking changes in the trend of the specular reflectivity accompanied by the rise of Yoneda off-specular scattering.

The analysis of these different signals indicated the presence of low-density regions of the SLB that are curved and protrude towards the bulk solvent. Altogether we show how SLBs can be efficiently used as models of the IMM, as they can also reproduce curved membrane regions. We also confirmed experimentally the central role of the CL with C18 acyl chain and Ca^{2+} ions in favouring membrane curvature and correct folding of the IMM. This evidence paves the way for the use of CL-containing SLBs to investigate membrane curvature also with other complementary techniques such as AFM and fluorescence microscopy.

CRediT authorship contribution statement

Alessandra Luchini: Writing – original draft, Project administration, Formal analysis, Conceptualization. **Yuri Gerelli:** Writing – review & editing, Conceptualization. **Philipp Gutfreund:** Writing – review & editing, Formal analysis. **Giovanna Fragneto:** Writing – review & editing, Conceptualization. **Luigi Paduano:** Writing – review & editing. **Giuseppe Vitiello:** Writing – review & editing, Conceptualization.

Declaration of competing interest

The authors declare that they have no known competing financial interests or personal relationships that could have appeared to influence the work reported in this paper.

Data availability

Data will be made available on request.

Acknowledgements

The authors thank the ILL for award of beamtime (DOI: 10.5291/ILL-DATA.9-13-685) and use of support facilities within the Partnership for Soft Condensed Matter.

Appendix A. Supplementary material

Supplementary material related to this article can be found online at https://doi.org/10.1016/j.molliq.2024.123973.

References

[1] E. Mileykovskaya, W. Dowhan, Cardiolipin membrane domains in prokaryotes and eukaryotes, Biochim. Biophys. Acta, Biomembr. 1788 (10) (2009) 2084–2091, https://doi.org/10.1016/j.bbamem.2009.04.003, includes Special Section: Cardiolipin.

[2] T. Harayama, H. Riezman, Understanding the diversity of membrane lipid composition, Nat. Rev. Mol. Cell Biol. 19 (2018) 281–296, https://doi.org/10.1038/nrm.2017.138.

[3] G. van Meer, D. Voelker, G. Feigenson, Membrane lipids: where they are and how they behave, Nat. Rev. Mol. Cell Biol. 9 (2) (2008) 112–124, https://doi.org/10.1038/nrm2330.

[4] K.C. Huang, R. Mukhopadhyay, N.S. Wingreen, A curvature-mediated mechanism for localization of lipids to bacterial poles, PLoS Comput. Biol. 2 (2006) 1–8, https://doi.org/10.1371/journal.pcbi.0020151.

[5] N. Ikon, R.O. Ryan, Cardiolipin and mitochondrial cristae organization, Biochim. Biophys. Acta, Biomembr. 1859 (6) (2017) 1156–1163, https://doi.org/10.1016/j.bbamem.2017.03.013.

[6] G. Paradies, V. Paradies, F.M. Ruggiero, G. Petrosillo, Role of cardiolipin in mitochondrial function and dynamics in health and disease: molecular and pharmacological aspects, Cells 8 (7) (2019), https://doi.org/10.3390/cells8070728.

[7] I.K. Jarsch, F. Daste, J.L. Gallop, Membrane curvature in cell biology: an integration of molecular mechanisms, J. Cell Biol. 214 (4) (2016) 375–387, https://doi.org/10.1083/jcb.201604003.

[8] S.M. Claypool, Cardiolipin, a critical determinant of mitochondrial carrier protein assembly and function, Biochim. Biophys. Acta, Biomembr. 1788 (10) (2009) 2059–2068, https://doi.org/10.1016/j.bbamem.2009.04.020.

[9] M.M. Elmer-Dixon, Z. Xie, J.B. Alverson, N.D. Priestley, B.E. Bowler, Curvature-dependent binding of cytochrome C to cardiolipin, J. Am. Chem. Soc. 142 (46) (2020) 19532–19539, https://doi.org/10.1021/jacs.0c07301.

[10] J.B. McMillin, W. Dowhan, Cardiolipin and apoptosis, Biochim. Biophys. Acta, Mol. Cell Biol. Lipids 1585 (2) (2002) 97–107, https://doi.org/10.1016/S1388-1981(02)00329-3, Lipids in apoptosis.

[11] M. Falabella, H.J. Vernon, M.G. Hanna, S.M. Claypool, R.D. Pitceathly, Cardiolipin, mitochondria, and neurological disease, Trends Endocrinol. Metab. 32 (4) (2021) 224–237, https://doi.org/10.1016/j.tem.2021.01.006.

[12] S. Ghio, F. Kamp, R. Cauchi, A. Giese, N. Vassallo, Interaction of α-synuclein with biomembranes in Parkinson's disease — role of cardiolipin, Prog. Lipid Res. 61 (2016) 73–82, https://doi.org/10.1016/j.plipres.2015.10.005.

[13] R.N. Lewis, D. Zweytick, G. Pabst, K. Lohner, R. McElhaney, Calorimetric, X-ray diffraction, and spectroscopic studies of the thermotropic phase behavior and organization of tetramyristoyl cardiolipin membranes, Biophys. J. 92 (9) (2007) P3166–P3177, https://doi.org/10.1529/biophysj.106.094003.

[14] R.N. Lewis, R.N. McElhaney, The physicochemical properties of cardiolipin bilayers and cardiolipin-containing lipid membranes, Biochim. Biophys. Acta, Biomembr. 1788 (10) (2009) 2069–2079, https://doi.org/10.1016/j.bbamem.2009.03.014, includes Special Section: Cardiolipin.

[15] M. Dahlberg, Polymorphic phase behavior of cardiolipin derivatives studied by coarse-grained molecular dynamics, J. Phys. Chem. B 111 (25) (2007) 7194–7200, https://doi.org/10.1021/jp071954f.

[16] J.M. Seddon, R. Kaye, D. Marsh, Induction of the lamellar-inverted hexagonal phase transition in cardiolipin by protons and monovalent cations, Biochim. Biophys. Acta, Biomembr. 734 (2) (1983) 347–352, https://doi.org/10.1016/0005-2736(83)90134-7.

[17] J.D. Unsay, K. Cosentino, Y. Subburaj, A.J. García-Sáez, Cardiolipin effects on membrane structure and dynamics, Langmuir 29 (51) (2013) 15878–15887, https://doi.org/10.1021/la402669z.

[18] S. Köhler, G. Fragneto, J.-P. Alcaraz, A. Nelson, D.K. Martin, M. Maccarini, Nanostructural characterization of cardiolipin-containing tethered lipid bilayers adsorbed on gold and silicon substrates for protein incorporation, Langmuir 37 (30) (2021) 8908–8923, https://doi.org/10.1021/acs.langmuir.1c00119.

[19] E. Beltrán-Heredia, F.-C. Tsai, S. Salinas-Almaguer, F.J. Cao, P. Bassereau, F. Monroy, Membrane curvature induces cardiolipin sorting, Commun. Biol. 2 (225) (2019), https://doi.org/10.1038/s42003-019-0471-x9.

[20] A. Luchini, D. Cavasso, A. Radulescu, G. D'Errico, L. Paduano, G. Vitiello, Structural organization of cardiolipin-containing vesicles as models of the bacterial cytoplasmic membrane, Langmuir 37 (28) (2021) 8508–8516, https://doi.org/10.1021/acs.langmuir.1c00981.

[21] N. Khalifat, J.-B. Fournier, M.I. Angelova, N. Puff, Lipid packing variations induced by ph in cardiolipin-containing bilayers: the driving force for the cristae-like shape instability, Biochim. Biophys. Acta, Biomembr. 1808 (11) (2011) 2724–2733, https://doi.org/10.1016/j.bbamem.2011.07.013.

[22] K. Funai, S.A. Summers, J. Rutter, Reign in the membrane: how common lipids govern mitochondrial function, Curr. Opin. Cell Biol. 63 (2020) 162–173, https://doi.org/10.1016/j.ceb.2020.01.006, cell Signalling (2020).

[23] M. Schlame, M. Ren, Y. Xu, M.L. Greenberg, I. Haller, Molecular symmetry in mitochondrial cardiolipins, Chem. Phys. Lipids 138 (1) (2005) 38–49, https://doi.org/10.1016/j.chemphyslip.2005.08.002.

[24] C. Osman, D.R. Voelker, T. Langer, Making heads or tails of phospholipids in mitochondria, J. Cell Biol. 192 (1) (2011) 7–16, https://doi.org/10.1083/jcb.201006159.

[25] B.A. Wilson, A. Ramanathan, C.F. Lopez, Cardiolipin-dependent properties of model mitochondrial membranes from molecular simulations, Biophys. J. 117 (3) (2019) 429–444.

[26] F. Elías-Wolff, M. Lindén, A.P. Lyubartsev, E.G. Brandt, Curvature sensing by cardiolipin in simulated buckled membranes, Soft Matter 15 (2019) 792–802, https://doi.org/10.1039/C8SM02133C.

[27] K.J. Boyd, N.N. Alder, E.R. May, Buckling under pressure: curvature-based lipid segregation and stability modulation in cardiolipin-containing bilayers, Langmuir 33 (27) (2017) 6937–6946, https://doi.org/10.1021/acs.langmuir.7b01185.

[28] G. Fragneto, R. Delhom, L. Joly, E. Scoppola, Neutrons and model membranes: moving towards complexity, Curr. Opin. Colloid Interface Sci. 38 (2018) 108–121, https://doi.org/10.1016/j.cocis.2018.10.003, Biological Colloids and Interfaces.

[29] R. Campbell, H. Wacklin, I. Sutton, R. Cubitt, G. Fragneto Figaro, The new horizontal neutron reflectometer at the ill, Eur. Phys. J. Plus 126 (2011) 107, https://doi.org/10.1140/epjp/i2011-11107-8.

[30] L.G. Parratt, Surface studies of solids by total reflection of X-rays, Phys. Rev. 95 (1954) 359–369, https://doi.org/10.1103/PhysRev.95.359.

[31] N. Kučerka, F.A. Heberle, J. Pan, J. Katsaras, Structural significance of lipid diversity as studied by small angle neutron and X-ray scattering, Membranes 5 (3) (2015) 454–472, https://doi.org/10.3390/membranes5030454.

[32] A.I. Greenwood, S. Tristram-Nagle, J.F. Nagle, Partial molecular volumes of lipids and cholesterol, Chem. Phys. Lipids 143 (1) (2006) 1–10, https://doi.org/10.1016/j.chemphyslip.2006.04.002.

[33] A. Hafner, P. Gutfreund, B.P. Toperverg, A.O.F. Jones, J.P. de Silva, A. Wildes, H.E. Fischer, M. Geoghegan, M. Sferrazza, Combined specular and off-specular reflectometry: elucidating the complex structure of soft buried interfaces, J. Appl. Crystallogr. 54 (3) (2021) 924–948, https://doi.org/10.1107/S1600576721003575.

[34] M.M. Elmer-Dixon, J. Hoody, H.B.B. Steele, D.C. Becht, B.E. Bowler, Cardiolipin preferentially partitions to the inner leaflet of mixed lipid large unilamellar vesicles, J. Phys. Chem. B 123 (43) (2019) 9111–9122, https://doi.org/10.1021/acs.jpcb.9b07690.

[35] Y. Yoneda, Anomalous surface reflection of X rays, Phys. Rev. 131 (5) (1963) 2010.

[36] M. Sathappa, N.N. Alder, The ionization properties of cardiolipin and its variants in model bilayers, Biochim. Biophys. Acta, Biomembr. 1858 (6) (2016) 1362–1372, https://doi.org/10.1016/j.bbamem.2016.03.007.

[37] E.R. Pennington, K. Funai, D.A. Brown, S.R. Shaikh, The role of cardiolipin concentration and acyl chain composition on mitochondrial inner membrane molecular organization and function, Biochim. Biophys. Acta, Mol. Cell Biol. Lipids 1864 (7) (2019) 1039–1052, https://doi.org/10.1016/j.bbalip.2019.03.012.

[38] C. Fernandez-Sanz, S. De la Fuente, S.-S. Sheu, Mitochondrial Ca2+ concentrations in live cells: quantification methods and discrepancies, FEBS Lett. 593 (13) (2019) 1528–1541, https://doi.org/10.1002/1873-3468.13427.

[39] A. Rasola, P. Bernardi, Mitochondrial permeability transition in Ca2+-dependent apoptosis and necrosis, Cell Calcium 50 (3) (2011) 222–233, https://doi.org/10.1016/j.ceca.2011.04.007, special issue on Ca2+ signaling mechanisms of cell survival and cell death.